

UC San Diego

UC San Diego Previously Published Works

Title

Prediction of Maternal and Fetal Pharmacokinetics of Dolutegravir and Raltegravir Using Physiologically Based Pharmacokinetic Modeling

Permalink

<https://escholarship.org/uc/item/77v831k5>

Journal

Clinical Pharmacokinetics, 59(11)

ISSN

0312-5963

Authors

Liu, Xiaomei I
Momper, Jeremiah D
Rakhmanina, Natella Y
[et al.](#)

Publication Date

2020-11-01

DOI

10.1007/s40262-020-00897-9

Peer reviewed



Prediction of Maternal and Fetal Pharmacokinetics of Dolutegravir and Raltegravir Using Physiologically Based Pharmacokinetic Modeling

Xiaomei I. Liu¹ · Jeremiah D. Momper² · Natella Y. Rakhmanina^{1,3} · Dionna J. Green⁴ · Gilbert J. Burckart⁵ · Tim R. Cressey^{6,7,8} · Mark Mirochnick⁹ · Brookie M. Best² · John N. van den Anker^{1,10} · André Dallmann^{10,11}

© Springer Nature Switzerland AG 2020

Abstract

Background Predicting drug pharmacokinetics in pregnant women including placental drug transfer remains challenging. This study aimed to develop and evaluate maternal–fetal physiologically based pharmacokinetic models for two antiretroviral drugs, dolutegravir and raltegravir.

Methods Physiologically based pharmacokinetic models were built with the Open Systems Pharmacology software suite (PK-Sim[®]/MoBi[®]). Different approaches to inform placental drug transfer were applied and compared. Model performance was evaluated using in vivo dolutegravir and raltegravir maternal plasma concentrations during the second and third trimesters and umbilical vein concentrations at delivery. All clinical in vivo data were obtained from the International Maternal Pediatric and Adolescent AIDS Clinical Trials (IMPAACT) Network P1026s study.

Results The physiologically based pharmacokinetic models successfully predicted plasma concentration–time profiles of dolutegravir and raltegravir in the second and third trimesters and predicted pharmacokinetic parameters fell mostly within a 1.33-fold error range. Predicted umbilical vein concentrations of dolutegravir were in reasonable agreement with in vivo data but were sensitive to changes in the placental partition coefficient and transplacental clearance.

Conclusions Maternal–fetal physiologically based pharmacokinetic modeling reliably predicted maternal pharmacokinetics of dolutegravir and raltegravir during pregnancy. For the fetal pharmacokinetics, data on the unbound fraction of highly protein-bound dolutegravir have proven to be important to adequately capture changes in total clearance in silico. More research efforts, along with clinical data, are needed to verify the predictions of fetal pharmacokinetics of antiretroviral drugs. Overall, the findings suggest that it may be possible to use physiologically based pharmacokinetic models to assess the disposition of antiretroviral drugs in pregnant women and their fetuses.

Electronic supplementary material The online version of this article (<https://doi.org/10.1007/s40262-020-00897-9>) contains supplementary material, which is available to authorized users.

✉ Xiaomei I. Liu
rph5862@gmail.com

¹ Division of Clinical Pharmacology, Children’s National Hospital, Washington, DC, USA

² Skaggs School of Pharmacy and Pharmaceutical Sciences, University of California San Diego, La Jolla, CA, USA

³ Elizabeth Glaser Pediatric AIDS Foundation, Washington, DC, USA

⁴ Office of Pediatric Therapeutics, US Food and Drug Administration, Silver Spring, MD, USA

⁵ Office of Clinical Pharmacology, US Food and Drug Administration, Silver Spring, MD, USA

⁶ PHPT/IRD 174, Faculty of Associated Medical Sciences, Chiang Mai University, Chiang Mai, Thailand

⁷ Department of Immunology and Infectious Diseases, Harvard T.H. Chan School of Public Health, Boston, MA, USA

⁸ Department of Molecular and Clinical Pharmacology, University of Liverpool, Liverpool, UK

⁹ Boston University, School of Medicine, Boston, MA, USA

¹⁰ Division of Pediatric Pharmacology and Pharmacometrics, University of Basel Children’s Hospital, Basel, Switzerland

¹¹ Clinical Pharmacometrics, Bayer, Leverkusen, Germany

Key Points

Maternal pharmacokinetics of dolutegravir and raltegravir in the second and third trimester of pregnancy were adequately predicted by the presented physiologically based pharmacokinetic (PBPK) models.

Fetal pharmacokinetics were predicted by integrating information on placental transfer generated exclusively by *in vitro* and *in silico* techniques in the PBPK models.

The findings on enzyme induction and placental transfer kinetics could be conceptualized to other drugs with similar physicochemical profile and, once thoroughly corroborated, used to support informed decision making in pregnant women.

1 Introduction

The recommendation to provide all pregnant women living with human immunodeficiency virus (HIV) with antiretroviral therapy (ART) has had a major impact on the prevention of vertical transmission of HIV in the USA and globally. The incidence rate for perinatally acquired HIV infection in the USA has decreased from over 5% in 2002 to about 2% in 2013 and to 53 cases in 2015 [1, 2]. The goal of the US Centers for Disease Control and Prevention is the complete elimination of perinatal HIV transmission [3]. Perinatal HIV infection still persists globally because of challenges with timely identifying HIV infection and maintaining suppressive ART throughout pregnancy, postpartum, and throughout breastfeeding. Providing efficacious ART to pregnant women is also challenging as physiologic changes during pregnancy can considerably affect the pharmacokinetics of antiretroviral drugs (ARVs). Indeed, a number of ARVs require a dose adjustment during pregnancy or are not recommended for use in pregnant women because of decreased plasma concentrations or fetal risks [4].

The integrase strand transfer inhibitors are recommended as first-line ART agents in ARV-naïve pregnant women [5]. Their initiation in late pregnancy has also been reported to rapidly achieve viral suppression by the time of delivery [6]. A recent report of the association between dolutegravir (DTG) use at the time of conception and a higher risk of neural tube birth defects in newborns has led to the change in the global and US guideline regarding DTG use in women of child-bearing potential, but still recommending the use of DTG during the second and third trimester of pregnancy [7, 8]. Physiological alterations in pregnancy may lead to

reduced maternal plasma concentrations of DTG and raltegravir (RAL), which increases the risks of viremia and vertical transmission of HIV. Understanding the pharmacokinetics of ARVs in pregnant women facilitates optimal dosing of ART and prevention of viremia and vertical transmission of HIV.

Physiologically based pharmacokinetic (PBPK) modeling is a promising approach to investigate the pharmacokinetics of xenobiotics in special populations where clinical trials are difficult to conduct, such as pregnant women and their fetuses. Physiologically based pharmacokinetic models are mechanistic models mapping the compartmental model structure to the circulatory system in a biologically plausible manner and integrating extensive information on the anatomy and physiology of the organism as well as physicochemical properties of the xenobiotic. While some pregnancy PBPK models have been previously reported [9], they are still not considered qualified for use in pregnancy because of limited experience. This study aimed to build a maternal–fetal PBPK model for DTG and RAL to predict their PK profiles in pregnant women during the second and third trimesters, as well as in their fetuses at delivery. This study presents a new process to parameterize unknown key parameters describing placental transfer (specifically, the transplacental clearance and drug partitioning between the fetus and the mother in the placenta) by combining recently proposed *in silico* techniques relying exclusively on *in vitro* information; additionally, drug partitioning between the fetus and the mother was estimated according to more conventional approaches and the results obtained from these methods were compared with clinical data. Predicted PK profiles were evaluated through comparison with *in vivo* data obtained from the International Maternal Pediatric and Adolescent AIDS Clinical Trials (IMPAACT) Network P1026s study (trial number: NCT00042289).

2 Materials and Methods

2.1 Software

Physiologically based pharmacokinetic models were developed using the open source software tool Open Systems Pharmacology (OSP) version 8.0 (<https://www.open-systems-pharmacology.org/>), which makes formerly commercial software PK-Sim[®] and MoBi[®] available as freeware under the GPLv2 License. All source code and the herein developed models will be made publicly available on GitHub (accessible via www.open-systems-pharmacology.org). WebPlotDigitizer (<https://automeris.io/WebPlotDigitizer/>) was used to extract data from published figures and convert them into digital format. The open source software PaDEL-Descriptor [10] was used to estimate molecular descriptors

of DTG and RAL and the free software R (version 3.4.1, R Foundation for Statistical Computing, Vienna, Austria; <https://www.r-project.org>) was used for non-compartmental analysis and graphics creation.

2.2 General Workflow

The workflow for the development of the pregnancy PBPK model has been previously described in detail [11] and is schematically shown in Fig. S1 of the Electronic Supplementary Material (ESM). Briefly, a PBPK model was initially developed for a virtual non-pregnant population and evaluated by comparing simulation results with the observed *in vivo* pharmacokinetic data in non-pregnant subjects reported in the comparison studies. Thereafter, the non-pregnant PBPK model was translated to pregnancy by substituting the standard model structure with the pregnancy structure and parametrizing the model for the respective gestational age as described before [11]. Pharmacokinetic predictions in pregnant women were evaluated by comparison with *in vivo* pharmacokinetic data obtained from clinical trials of IMPAACT P1026s.

2.3 Development of Physiologically Based Pharmacokinetic (PBPK) Pregnancy Models

2.3.1 Dolutegravir

Dolutegravir is dosed at 50 mg once daily as an orally administered tablet in both pregnant and non-pregnant treatment-naïve and treatment-experienced adult patients without integrase strand transfer inhibitor resistance. Dolutegravir is primarily eliminated by metabolism through various enzymes including uridine 5'-diphospho-glucuronosyltransferase (UGT) 1A1, UGT1A3, UGT1A9, and cytochrome P450 (CYP) 3A4 (~51%, ~2.8%, ~5.5%, and ~21% of the dose, respectively [12]). In the developed model, the contribution of UGT1A3 and 1A9 to total glucuronidation was combined into the biotransformation pathway mediated by UGT1A1. Finally, to obtain dose fractions summing up to 1.0, the dose fraction metabolized via UGT1A1 was increased to 0.79 based on the assumption that the reported value (0.51) may be underestimated owing to hydrolyzation and back conversion of the glucuronide to DTG in the feces, as discussed elsewhere [12]. The PBPK model input parameters for DTG are listed in Table 1.

In the pregnancy PBPK model, physiologic parameters were adjusted to the respective stage of pregnancy as described previously [13]. Additionally, the reference concentrations of UGT1A1 and CYP3A4 (quantifying the concentrations of these enzymes in the model) were increased to reflect induction of these enzymes. Specifically, CYP3A4 reference concentration was increased by a factor of 1.60

in the second and third trimesters and UGT1A1 reference concentration by a factor of 1.75 in the second trimester and 1.92 in the third trimester [14, 15]. The fraction unbound of DTG, averaging 0.0070 in non-pregnant subjects, [16] was also adjusted based on the albumin level measured in the herein investigated study subjects. Specifically, the mean albumin level measured in the second trimester, third trimester, and 6–12 weeks postpartum was 34.4 g/L, 32.8 g/L, and 41.4 g/L, respectively. Using a previously presented scaling approach [13], these measurements resulted in a fraction unbound of 0.0084 and 0.0088 in the second and third trimester, respectively. Additional information on model development and translation to pregnancy can be found in the ESM.

Pharmacokinetic simulations in the non-pregnant population were evaluated by comparison with *in vivo* data obtained from eight clinical studies reported in the literature that investigated the pharmacokinetics of DTG in a total of 22 different groups of non-pregnant subjects after single and multiple oral administrations of 2–100 mg as a granule suspension or 50 mg as a tablet in a fasted or fed state [17–26]. In pregnant women, the pharmacokinetics were predicted in two different gestational age groups of non-laboring pregnant women in the second trimester (median gestational age [range]: 23.5 [20–25] weeks) and third trimester (median gestational age [range]: 33 [30–37] weeks), and in women in labor (median gestational age [range]: 38 [35–42] weeks). Drug concentrations in the blood plasma of the umbilical vein were predicted in the laboring pregnant women group.

2.3.2 Raltegravir

Raltegravir is dosed at 400 mg twice daily or 1200 mg once daily as orally administered tablets in both pregnant and non-pregnant treatment-naïve and treatment-experienced adult patients. Raltegravir is primarily eliminated by metabolism catalyzed by UGT1A1 and UGT1A9 (~70% and 11% of the administered dose, respectively [27]). Additionally, approximately 9% is eliminated unchanged through the kidneys [27]. The input parameters and their values for the RAL PBPK model are listed in Table 1. Additional information can be found in the ESM. The non-pregnant PBPK model for RAL was obtained from the OSP GitHub repository (<https://github.com/Open-Systems-Pharmacology/Raltegravir-Model/releases>) where an extensive description and evaluation of the model can be found.

In the pregnancy PBPK model, physiologic parameters and the reference concentrations of UGT1A1 were adjusted to the respective stage of pregnancy as described above. As no information on the effect of pregnancy on UGT1A9 could be found, this enzyme was not induced in the presented model. Similar to DTG, the fraction unbound of RAL, averaging 0.17 in non-pregnant adults, [28] was

Table 1 Summary of input data for physiologically based pharmacokinetic models in non-pregnant subjects

Parameter [unit]	Dolutegravir		Raltegravir	
	Value	References	Value	References
Molecular weight [g/mol]	419.38	Drugbank.ca	444.42	Drugbank.ca
Lipophilicity [log units]	0.98	Fitted ^a	0.58	Moss et al. [71]
p <i>K</i> _a (acid)	10.1	Drugbank.ca	6.67	Moss et al. [71]
Fraction unbound:				
Non-pregnant	7.0E−3	Clinical Pharmacology and Biopharmaceutics Review [16]	0.170	Laufer et al. [28]
Second trimester	8.4E−3	Calculated	0.198	Calculated
Third trimester	8.8E−3	Calculated	0.206	Calculated
Major binding protein	Albumin	Drugbank.ca	Albumin	Laufer et al. [28]
Solubility (at pH 7) [mg/L]	0.172 ^c ; 1.98 ^d ; 0.0252 ^e	Fitted ^a	8900 ^f	Moss et al. [72]
Intestinal permeability (transcellular) [cm/min]	0.05	Fitted ^a	1.71 × 10 ^{−5}	Fitted ^g
Model for estimating organ-to-plasma partition coefficients	Rogers and Rowland		Rogers and Rowland	
GFR fraction			1.0	Kassahun et al. [27]
<i>K</i> _{m-UGT1A1} [μM]	149	Reese et al. [12]	99	Kassahun et al. [27]
<i>V</i> _{max-UGT1A1} [nmol/min/mg]	7.34	Fitted ^a	2.74 ^d	Fitted ^g
<i>K</i> _{m-UGT1A9} [μM]			296	Kassahun et al. [27]
<i>V</i> _{max-UGT1A9} [nmol/min/mg]			1.63 ^d	Fitted ^g
CLspec/[CYP3A4 enzyme] [L/μmol/min]	0.05	Fitted ^a		

GFR glomerular filtration rate

^aValue simultaneously fitted to in vivo plasma concentration–time profiles of non-pregnant subjects and to the reported dose fractions metabolized [17–26]

^bSolubility for the suspension

^cSolubility for the tablet formulation administered in a fasted state

^dSolubility for the tablet formulation administered in a fed state

^eSolubility for the suspension

^fSolubility implemented as table: pH = 1–4, solubility = 40 mg/L; pH = 5, solubility = 120 mg/L; pH = 6, solubility = 980 mg/L; pH = 7, solubility = 8900 mg/L; pH = 8, solubility = 37,300 mg/L

^gValue fitted to in vivo pharmacokinetic data of non-pregnant subjects following oral administration [27, 73–77]

adjusted based on the mean albumin level measured in the second trimester, third trimester, and 6–12 weeks postpartum (34.1 g/L, 32.4 g/L, and 41.4 g/L, respectively), resulting in a fraction unbound of 0.198 and 0.206 in the second and third trimester, respectively. Additional information on model development and translation to pregnancy can be found in the ESM.

In pregnant women, the pharmacokinetics were predicted in two different gestational age groups of non-laboring pregnant women in the second trimester (median gestational age [range]: 23.5 [21–26] weeks) and the third trimester (median gestational age [range]: 34 [30–38] weeks), and in women in labor (median gestational age [range]: 38 [36–40] weeks). Drug concentrations in the blood plasma of the umbilical vein were predicted in the laboring pregnant women group.

2.3.3 Clinical In Vivo Data in Pregnant Women Living with Human Immunodeficiency Virus

The clinical in vivo data were from the IMPAACT network P1026s study. Intensive steady-state blood samples for PK assessment were collected in the second trimester (optional), third trimester, and postpartum, and single maternal and cord blood samples were collected at delivery. Further information can be found in Table S1 of the ESM. The performance of the PBPK model to predict drug concentrations in the umbilical cord was evaluated via comparison with clinical in vivo data collected at delivery. The protocol for this study was approved by the responsible institutional review boards. The IMPAACT P1026s study is an ongoing (trial number: NCT00042289), multicenter, phase IV prospective study and a part of the herein reported data has been previously

published [29, 30]. In addition, clinical PK data in pregnant women reported by Waitt et al. [31] and Blonk et al. [32] were used to evaluate the steady-state PK predictions of DTG around gestational week 31 and of RAL around gestational week 33, respectively.

2.4 Parameterization of Placental Transfer

Placental transfer kinetics of DTG and RAL was mathematically described as reported previously [33] (also described in detail in the ESM) and informed by *in silico* methods. Specifically, the transplacental clearance (D_{pl}) was estimated from the approach suggested by Zhang and Unadkat [34], which estimates the transplacental clearance from the permeability measured in Caco2 cell lines. For DTG, Caco2 cell permeability ($2.5E-6$ cm/s) was obtained from Griessinger et al. [35], resulting in a transplacental clearance of 0.43 L/min. For RAL, a Caco2 cell permeability of $7.3E-6$ cm/s was reported [36], resulting in a transplacental clearance of 1.24 L/min.

Four different methods were used to estimate the partition coefficient between the fetal intracellular space and the maternal blood plasma of the placenta in the model ($K_{fc:mp}$), in particular: (1) the “PK-Sim Standard” calculation method [37]; (2) the method proposed by Poulin and Theil [38, 39]; (3) the method proposed by Rodgers and Rowland [40, 41]; and (4) a quantitative structure–activity relationship (QSAR) model for the fetal–maternal blood concentration ratio, which was used as surrogate for $K_{fc:mp}$. The fetal–maternal blood concentration ratio was calculated according to the QSAR model suggested by Takaku et al. [42] which uses molecular weight, polar surface area, and maximum E-state of hydrogen atom in the compound to estimate the fetal–maternal blood concentration ratio. Using the open source software PaDEL-Descriptor [10], the polar surface area was estimated to be 95.9 \AA^2 and 147 \AA^2 for DTG and RAL, respectively; and maximum E-state of hydrogen atom in the compound was 0.93 and 0.82 for DTG and RAL, respectively. Physiological values required for calculating the partition coefficients according to the other three methods, e.g., tissue composition, are published elsewhere [13]. The values for $K_{fc:mp}$ calculated according to each of the four methods are listed in Table 2.

2.5 Parameterization of Placental Metabolism

In the model, the amount of CYP3A4, UGT1A1, and UGT1A9 in the fetal part of the placenta and the fetal body was informed based on reported data from previous studies that quantified the messenger RNA level of CYP3A4 [43] as well as protein levels and the activity of UGT1A1 [44, 45] in various human tissues, including the adult liver, placenta, and fetal liver. Further information can be found in the ESM.

Table 2 Values for the partition coefficient between the fetal intracellular space and the maternal blood plasma in the placenta ($K_{fc:mp}$) calculated according to different methods

Drug	Method			
	PK-Sim standard	Poulin and Theil	Rodgers and Rowland	QSAR
Dolutegravir	0.0085	0.43	0.04	0.40
Raltegravir	0.19	0.52	0.26	0.42

QSAR quantitative structure–activity relationship

Table 3 Enzymes amount included in fetal compartments of the physiologically based pharmacokinetic model

Tissue	Enzyme amount (μmol)		
	CYP3A4	UGT1A1	UGT1A9
Fetal part of the placenta	$3.98E-4$	0.06	NA
Fetus	0.12	0.03	0.024

CYP cytochrome P450, NA not available

The protein amounts listed in Table 3 were then incorporated into the pregnancy PBPK model. As discussed further below, the difference of fraction unbound between fetus and mother was not considered because of the high uncertainty in fetal protein binding.

2.6 Evaluation of PBPK Models

The PBPK models were evaluated through visual comparison of observed *in vivo* plasma concentration–time profiles with the concentrations simulated in non-pregnant subjects or predicted in pregnant women. Additional visual assessments included goodness-of-fit (GOF) and residuals vs time plots. Ratios of simulated to observed pharmacokinetic parameters were estimated and the number of ratios falling within a 1.33-fold error range (i.e., $0.75 \leq \text{ratio} \leq 1.33$) was given. An extensive evaluation of the non-pregnant PBPK model for RAL has been previously published on GitHub (<https://github.com/Open-Systems-Pharmacology/Raltegravir-Model>).

2.7 Sensitivity Analysis

Local sensitivity analyses were conducted to assess how the uncertainty in specific parameters propagates to the final model output (plasma concentration–time profiles in the second and third trimesters of pregnancy or at delivery). The following parameters were included in local (univariate) sensitivity analyses: UGT1A1 induction, the transplacental

clearance, and the gastric emptying time of the mother at delivery.

3 Results

3.1 Non-pregnant PBPK Models

3.1.1 Dolutegravir

The simulated plasma concentration–time profiles of DTG in non-pregnant populations following administration of the 50-mg tablet once daily in the fed state (i.e., the same

dosing regimen than in pregnant women) are shown in Fig. 1, while Fig. S2 of the ESM shows simulated plasma concentration–time profiles following other dosing regimens. The ratios of simulated to observed PK parameters in non-pregnant subjects are listed in Table 4 together with the absolute simulated and observed values. All simulated area under the concentration–time curve (AUC) values fell within a 1.33-fold error range. Eleven out of 13 (85%) maximum concentration (C_{max}) values fell within a 1.33-fold error range. Time to C_{max} (t_{max}) was somewhat less accurately simulated, but still 10 out of 13 (77%) simulated values fell within a 1.33-fold error range. This model was subsequently translated to pregnant women.

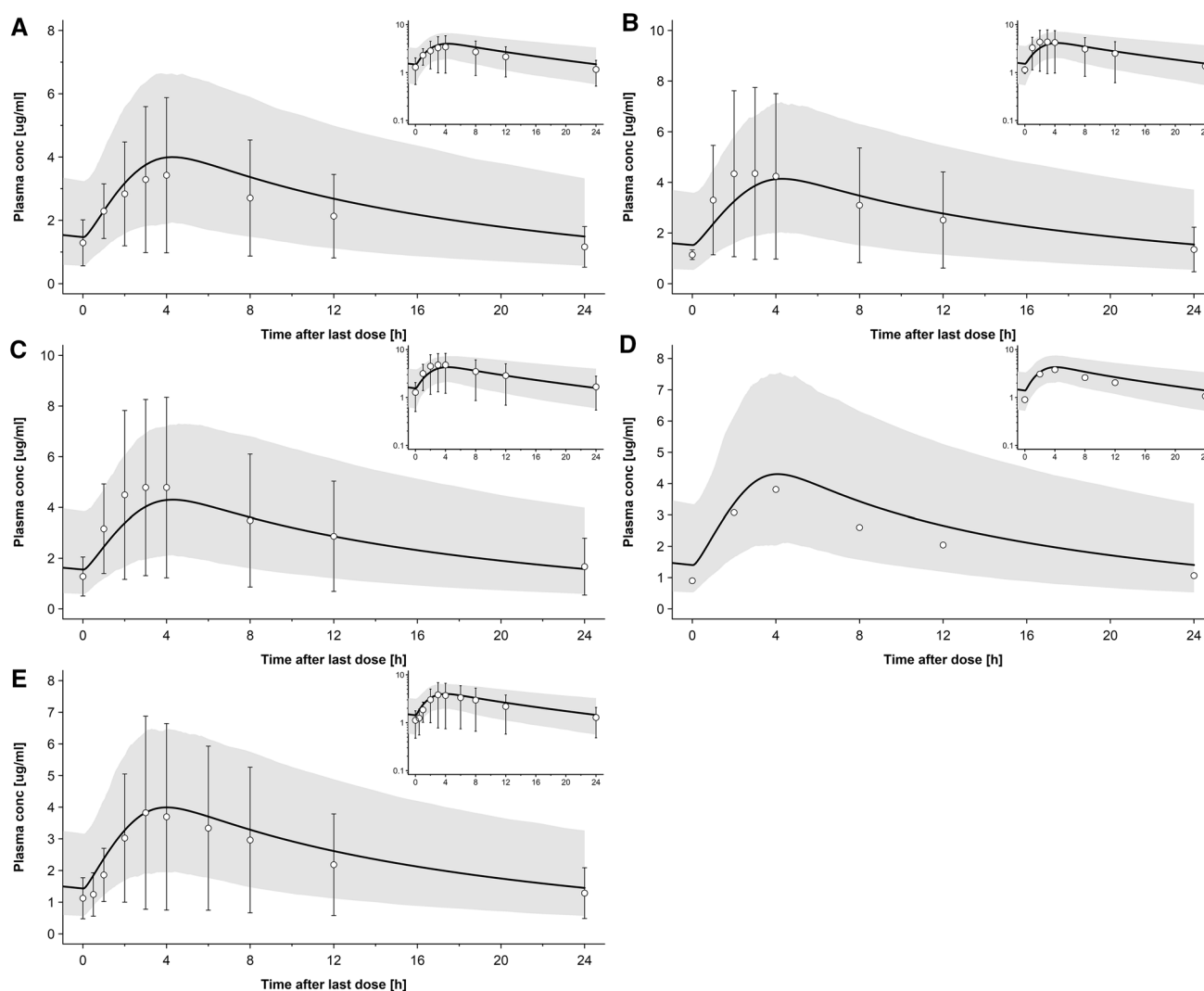


Fig. 1 Plasma concentration–time profiles of dolutegravir following oral administration once a day of 50 mg in a fed state in non-pregnant subjects. Circles represent observed in vivo data from the following studies: **a** Ford et al. [23]; **b** group 1 of the study from Johnson et al. [24]; **c** group 2 of the study from Johnson et al. [24]; **d** Wang

et al. [25]; **e** Song et al. [20]. The solid line represents the simulated plasma concentration in the respective population and the shaded area is the simulated 5th–95th percentile range. Semi-log scale figures are given as an inset figure in the top-right corners

Table 4 Comparison of simulated or predicted and observed pharmacokinetic parameters

	AUC _{0–t} [mg · h/L] ^a Simulated/observed (ratio)	C _{max} [mg/L] Simulated/observed (ratio)	t _{max} [h] Simulated/observed (ratio)
Dolutegravir			
<i>Non-pregnant women</i>			
Castellino study [17]	34.0/35.9 (0.95)	2.29/2.53 (0.86)	0.95/0.50 (1.90)
Dooley study, cohort 1 [18] (steady state)	39.0/36.1 (1.08)	2.91/2.65 (1.10)	2.25/1.5 (1.50)
Dooley study, cohort 2 [18] (steady state)	41.1/42.1 (0.98)	2.96/2.91 (1.02)	2.20/2.00 (1.10)
Ford study [23] (steady state)	63.1/52.5 (1.20)	4.00/3.43 (1.17)	4.25/4.00 (1.06)
Johnson 2014, cohort 1 (steady state) [24]	65.2/71.9 (0.91)	4.14/4.35 (0.95)	4.30/3.00 (1.43)
Johnson 2014, cohort 2 (steady state) [24]	67.4/71.9 (0.94)	4.30/4.78 (0.90)	4.30/3.50 (1.23)
Song 2012 (high fat meal) [21]	66.1/83.6 (0.79)	2.97/4.19 (0.71)	4.90/5.00 (0.98)
Song 2012 (low fat meal) [21]	59.8/66.7 (0.90)	2.83/3.81 (0.74)	4.00/3.00 (1.33)
Song 2012 (moderate fat meal) [21]	64.7/71.0 (0.91)	2.94/3.86 (0.76)	4.75/4.00 (1.19)
Song 2016 (moderate fat meal) [20] (steady state)	62.2/55.4 (1.12)	3.99/3.83 (1.04)	4.00/3.00 (1.33)
Song 2013 study [19] ^b	47.2/40.3 (1.17)	1.82/1.90 (0.96)	2.50/3.00 (0.83)
Weller study [22]	44.1/37.1 (1.19)	1.89/1.84 (1.03)	2.40/2.50 (0.96)
Wang 2019 [25]	63.8/51.62 (1.23)	4.30/3.81 (1.13)	4.10/4.00 (1.03)
<i>Pregnant women</i>			
Second trimester (steady state)	34.70/42.38 (0.82)	2.77/3.00 (0.92)	4.20/2.00 (2.10)
Third trimester (steady state)	31.91/47.59 (0.67)	2.57/3.00 (0.86)	4.20/4.00 (1.05)
Raltegravir			
<i>Non-pregnant women</i>			
Markowitz 2006 [75]	See OSP GitHub	See OSP GitHub	See OSP GitHub
Iwamoto 2009 [78]	8.86/7.96 (1.11)	3.04/2.24 (1.36)	0.80/1.00 (0.80)
Rhee 2014 [76]	8.66/4.90 (1.77)	3.10/1.28 (2.42)	0.75/1.50 (0.50)
Rhee 2014 [76]	9.13/8.53 (1.07)	3.11/2.22 (1.40)	0.75/2.00 (0.38)
Wenning 2009 [77]	8.99/12.25 (0.73)	3.12/3.82 (0.81)	0.75/1.50 (0.50)
Brainard 2011 (fasted state) ^b [79]	9.66/6.47 (1.49)	3.42/1.59 (2.15)	0.75/2.00 (0.38)
Brainard 2011 (high fat meal) ^b [79]	8.83/ 11.37 (0.78)	1.48/1.59 (0.93)	2.45/2.00 (1.23)
Brainard 2011 (moderate fat meal) ^b [79]	8.86/6.44 (1.38)	1.54/0.74 (2.08)	2.20/4.00 (0.55)
Brainard 2011 (low fat meal) ^b [79]	9.01/3.39 (2.66)	1.76/0.59 (2.98)	1.95/3.50 (0.56)
Taburet 2015 (moderate fat meal, group 1) ^c [80]	8.46/8.24 (1.03)	1.65/2.03 (0.82)	2.20/1.00 (2.20)
Taburet 2015 (moderate fat meal, group 2) ^c [80]	8.95/ 11.00 (0.81)	1.54/2.77 (0.56)	2.20/2.00 (1.10)
<i>Pregnant women</i>			
Second trimester (steady state)	4.10/3.90 (1.05)	0.834/0.67 (1.22)	2.55/2.00 (1.28)
Third trimester (steady state)	3.71/4.44 (0.84)	0.763/0.85 (0.89)	2.50/2.00 (1.25)

Data expressed as geometric mean values unless indicated otherwise

AUC_{0–t} area under the concentration–time curve from zero to the time point of the last observed plasma concentration (in case of multiple-dose studies, time refers to the time after last dose), AUC_{0–∞} area under the concentration–time curve from zero to infinity, C_{max} peak plasma concentration, t_{max} time at which peak plasma concentration is reached

^aAUC_{0–t} was used in the studies by Dooley et al. [18], Ford et al. [23], Johnson et al. [24], Song et al. [20], Markowitz et al. [75], Brainard et al. [79], and Taburet et al. [80]; whereas AUC_{0–∞} was used in the studies by Castellino et al. [17], Song et al. [21], Song et al. [19], Weller et al. [22], Iwamoto et al. [78], Rhee et al. [76], and Wenning et al. [77]

^bData expressed as arithmetic mean values

^cData expressed as median values

3.1.2 Raltegravir

An extensive evaluation of the non-pregnant PBPK model for RAL can be found in the model repository on GitHub (<https://github.com/Open-Systems-Pharmacology/Raltegravir-Model>); here, only a limited number of results is

shown. The simulated plasma concentration–time profiles of RAL in non-pregnant populations following administration of a 400-mg tablet twice daily in the fed state (i.e., the same dosing regimen as in pregnant women) are shown in Fig. 2. In addition, Fig. S3 of the ESM shows simulated plasma concentration–time profiles following other dosing

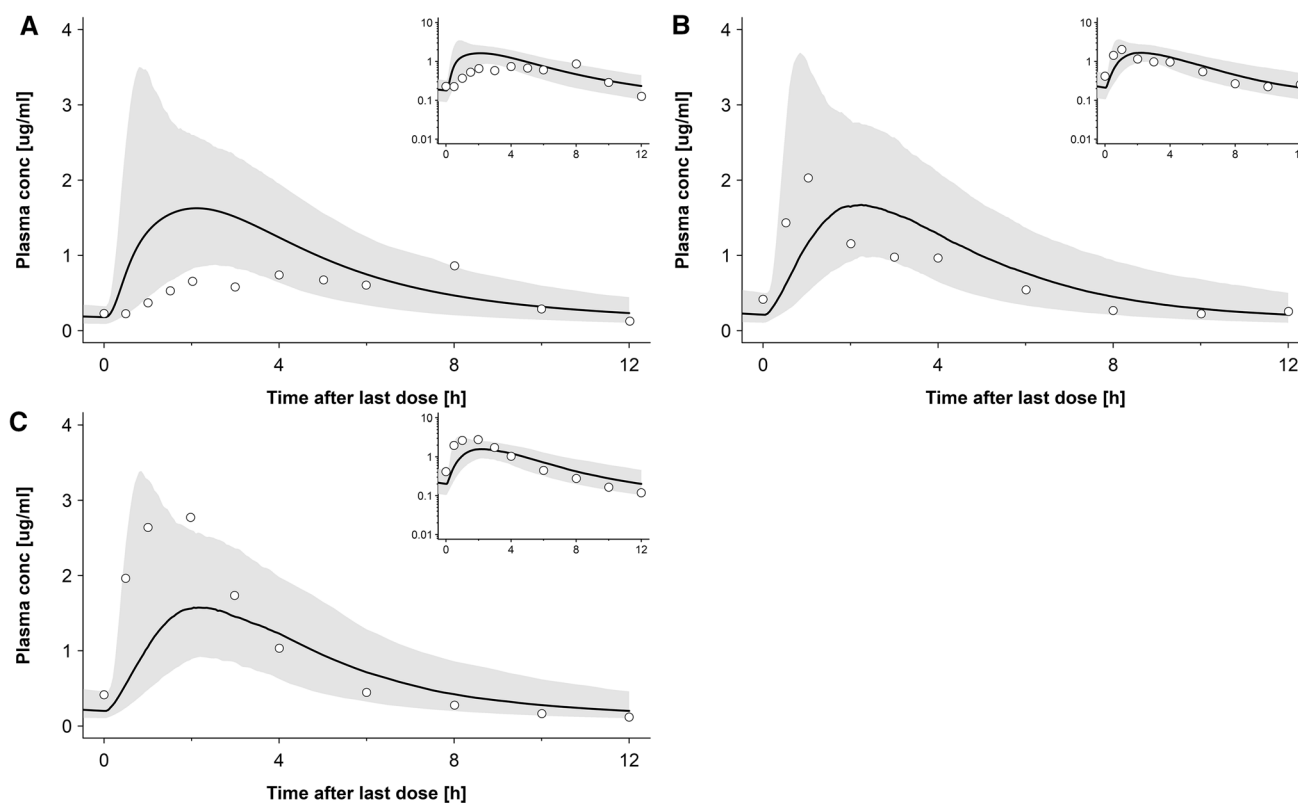


Fig. 2 Plasma concentration–time profiles of raltegravir following oral administration twice a day of 400 mg with a moderate-fat meal in non-pregnant subjects. Circles represent observed in vivo data from the following studies: **a** Brainard et al. [79]; **b** group 1 of the study from Taburet et al. [80]; **c** group 2 of the study from Taburet et al.

regimens. The ratios of simulated to observed PK parameters in non-pregnant subjects are listed in Table 4 together with the absolute simulated and observed values. Five out of ten (50%) simulated AUC values fell within a 1.33-fold error range (i.e., $0.75 \leq \text{ratio} \leq 1.33$). For C_{\max} and t_{\max} , three out of ten (30%) simulated values were within this range. While there were some difficulties in describing the data of a few clinical studies, the model was overall deemed adequately to describe RAL pharmacokinetics when also considering additional studies with different posology (see Fig. S3 of the ESM and additional information available on <https://github.com/Open-Systems-Pharmacology/Raltegravir-Model>). Hence, this model was subsequently translated to pregnant women.

3.2 Pregnancy PBPK Models in the Second and Third Trimester

3.2.1 Dolutegravir

The predicted DTG plasma concentration–time profiles in the second and third trimesters of pregnancy are shown in

[80]. The solid line represents the simulated plasma concentration in the respective population and the shaded area is the simulated 5th–95th percentile range. Semi-log scale figures are given as an inset figure in the top-right corners

Fig. 3 and in Fig. S5 of the ESM with clinical data reported by other research groups. Figure 4 shows the GOF plot for the model-predicted DTG plasma concentrations in non-pregnant and pregnant women. All but two out of 16 (87.5%) geometric mean DTG concentrations were predicted within a 2-fold error range. The absolute values as well as ratios of predicted-to-observed area under the concentration–time curve in the last dosing interval (AUC_{τ}), C_{\max} , and t_{\max} in the pregnant populations are listed in Table 4. The AUC_{τ} of the second trimester and C_{\max} of the second and third trimesters were predicted within a 1.33-fold error range. The AUC_{τ} in the third trimester was predicted within a 1.5-fold error range; similar to simulations in non-pregnant subjects, t_{\max} was less accurately predicted in the second trimester, but again in the 1.33-fold error range in the third trimester. Table S2 of the ESM provides an overview of additional pharmacokinetic parameters simulated in non-pregnant and predicted in pregnant populations. Variability was reasonably described by the model; specifically, the predicted 5th–95th percentile range contained 76% of all observed concentration values in the second trimester and 69% of all observed concentration values in the third trimester.

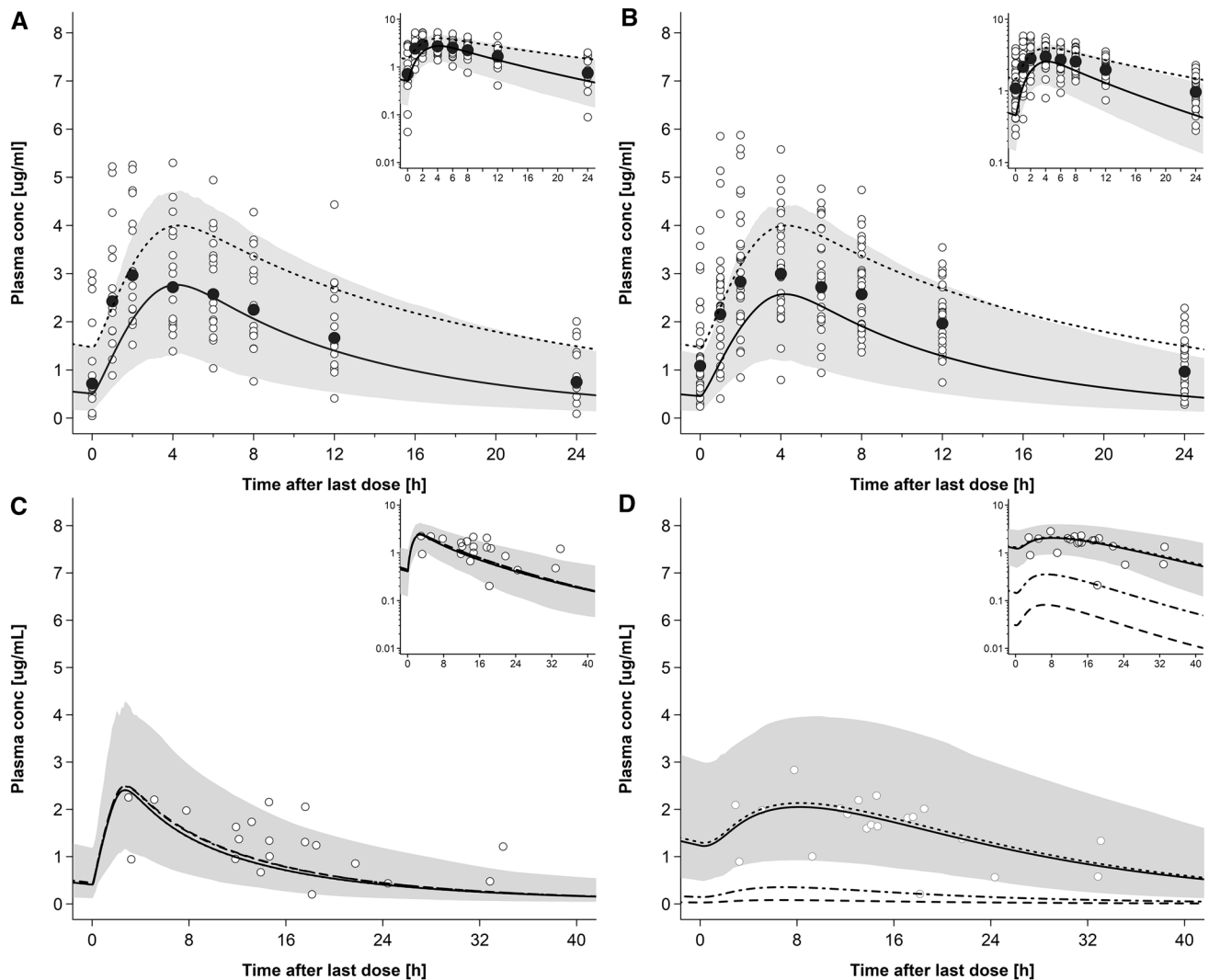
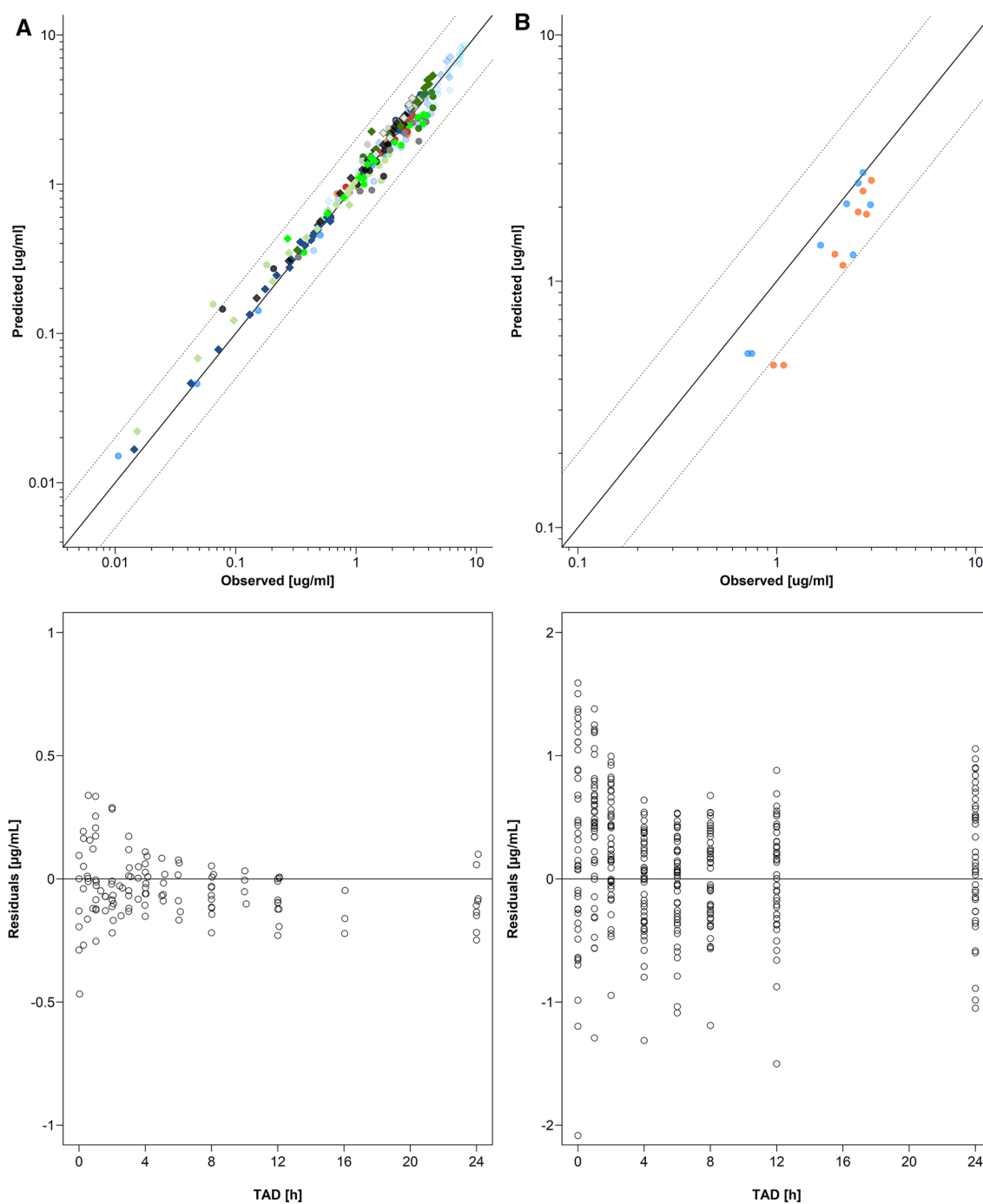


Fig. 3 Plasma concentration–time profiles of dolutegravir following oral administration of 50 mg once a day in pregnant women. Semi-log scale figures are given as an inset figure in the top-right corners. Observed steady-state *in vivo* data were taken from an *in vivo* study of IMPAACT P1026 [29]. **a** Dolutegravir 50 mg once a day in pregnant women in the second trimester. Empty circles and black circles represent individual concentrations and geometric mean concentration, respectively, taken from an *in vivo* study of IMPAACT P1026 [29]. The solid line represents the predicted geometric mean concentration and the shaded area the predicted 5th–95th percentile range; the dotted line represents the predicted geometric mean concentration of the non-pregnant population; **b** dolutegravir 50 mg once a day in pregnant women in the third trimester. Empty circles and black circles represent individual concentrations and geometric mean concentration, respectively, taken from an *in vivo* study of IMPAACT P1026 [29]. The solid line represents the predicted geometric mean concentration and the shaded area the predicted 5th–95th percentile range; the dotted line represents the predicted geometric mean concentration of the non-pregnant population; **c** dolutegravir 50 mg once a day in pregnant women with an average gestational age of 38 weeks at delivery. Empty circles represent individual concentration data in the maternal plasma taken from an *in vivo* study of IMPAACT P1026

[29]; the lines represent the predicted geometric mean concentration in the maternal plasma using different placental partition coefficients calculated by different methods; the solid line represents the quantitative structure–activity relationship (QSAR) method; the dotted line represents the Poulin and Theil method; the dash-dot line represents the Rodgers and Rowland method; and the dash line represents the PK-Sim standard method. The shaded area represents the predicted 5th–95th percentile range obtained from the model incorporating the QSAR-informed placental partition coefficient. **d** Dolutegravir 50 mg once a day in pregnant women with an average gestational age of 38 weeks at delivery. Empty circles represent individual concentration data in the umbilical vein taken from an *in vivo* study of IMPAACT P1026; [29] the lines represent the predicted geometric mean concentration in the umbilical vein using different placental partition coefficients calculated by different methods: the solid line represents the QSAR method; the dotted line represents Poulin and Theil method; the dash-dot line represents the Rodgers and Rowland method; and the dash line represents the PK-Sim standard method. The shaded area presents the predicted 5th–95th percentile range obtained from the model incorporating the QSAR-informed placental partition coefficient



3.2.2 Raltegravir

The predicted RAL plasma concentration–time profiles in the second and third trimesters of pregnancy are shown in Fig. 5 and in Fig. S5 of the ESM with clinical data reported by other research groups. Figure 6 shows the GOF plot for the model-predicted RAL plasma concentrations in non-pregnant and pregnant women with the residuals vs time. All but 1 out of 14 (92.9%) geometric mean RAL concentrations in pregnant populations were predicted

within a 2-fold error range. The observed and predicted values for AUC_{tau} , C_{max} , and t_{max} as well as their ratios are listed in Table 4. These geometric mean PK parameters were all predicted within a 1.33-fold error range in the second and third trimesters. Table S2 of the ESM provides an overview of additional PK parameters simulated in non-pregnant and predicted in pregnant populations. Variability was underestimated by the model; specifically, the predicted 5th–95th percentile range contained only 64% of all observed concentration values in the second

Fig. 4 Goodness-of-fit (GOF) and residuals vs time plots of dolutegravir concentrations in non-pregnant subjects (a) and pregnant women (b). The solid line represents the line of identity and the dotted lines the two-fold error range. **a** Upper plot: GOF plot of geometric mean dolutegravir concentrations in non-pregnant populations. Single-dose study: blue circles indicate the study by Castellino et al. (20-mg single dose) [17]; green circles indicate the study by Song et al. (50-mg single dose) [19]; light blue circles indicate the high-fat meal group in the study by Song et al. (50-mg single dose) [21]; black circles indicate the study by Weller et al. (50-mg single dose) [22]; bright green circles indicate the moderate-fat meal group in the study by Song et al. (50-mg single dose) [21]; gray circles indicate the low-fat meal group in the study by Song et al. (50-mg single dose) [21]. Multiple-dose study: dark blue circles indicate the study by Ford et al. (50 mg once daily) [23]; orange circles indicate the group 1 in the study by Dooley et al. (50 mg once daily) [18]; red circles indicate the group 2 in the study by Dooley et al. (50 mg once daily) [18]; dark green circles indicate the group 1 in the study by Johnson et al. (50 mg once daily) [24]; sky blue circles indicate the group 2 in the study by Johnson et al. (50 mg once daily) [24]; light grey circles indicate the study by Song et al. (50 mg once daily) [20]; yellow circles indicate the study by Wang et al. (50 mg once daily) [25]. Lower plot: residuals vs time plot of dolutegravir in a non-pregnant population. Empty circles represent the geometric mean concentrations of non-pregnancy reference studies. **b** Upper plot: GOF plot of dolutegravir in the pregnant population. Blue circles indicate geometric mean concentrations in the second trimester and orange circles indicate geometric mean concentrations in the third trimester. Lower plot: residuals vs time plot of dolutegravir in the pregnant population. Empty circles represent the individual concentrations in the second and third trimesters

trimester and 55% of all observed concentration values in the third trimester.

3.3 Pregnancy PBPK Models for Delivery

3.3.1 Dolutegravir

Maternal and umbilical cord plasma concentrations of DTG predicted at delivery are shown in Fig. 3c, d, respectively. For the PBPK model incorporating the QSAR-informed $K_{fc:mp}$, fourteen out of 20 maternal samples at delivery fell within the 2-fold error range of the predicted mean concentration, and 8/20 maternal samples fell within the 1.5-fold error range. Seventeen out of 20 cord samples fell within the 2-fold error range of the predicted mean concentration and 11/20 cord samples fell within the 1.5-fold error range. The predicted steady-state exposure was higher in the fetus compared with the mother; specifically, the predicted geometric AUC_{tau} was 40.99 mg h/L in the umbilical vein and 26.84 mg h/L in the maternal plasma.

3.3.2 Raltegravir

Maternal and umbilical cord plasma concentrations of DTG predicted at delivery are shown in Fig. 5c, d, respectively. For the PBPK model incorporating the QSAR-informed

$K_{fc:mp}$, five out of 24 maternal samples fell within the 2-fold error range of the predicted mean and 7/23 fetal samples fell within the 2-fold error (one fetal sample was missing). The predicted steady-state exposure was higher in the fetus compared with the mother; specifically, the predicted geometric AUC_{tau} was 4.73 mg h/L in the fetus and 3.16 mg h/L in the maternal plasma.

3.4 Sensitivity Analyses

Local sensitivity analyses results are shown in Figs. S4, S6, and S7 of the ESM. The sensitivity analysis of UGT1A1 induction shown in Fig. S4 indicated that, within the tested range, UGT1A1 induction had a moderate influence on the predicted pharmacokinetics of DTG and RAL during pregnancy. The sensitivity analysis for the placenta diffusion clearance shown in Fig. S6 suggests that it was a sensitive model parameter for DTG but not for RAL. Although no sensitivity analysis was conducted for $K_{fc:mp}$, Figs. 3d and 5d show the predicted pharmacokinetics in the umbilical vein when different values for $K_{fc:mp}$ are incorporated into the model. Further sensitivity analyses on the gastric emptying time of the mother are shown in Fig S7, indicating that a prolonged gastric emptying time slightly increases both maternal and fetal exposure.

4 Discussion

In this study, maternal–fetal PBPK models were developed for DTG and RAL and evaluated by comparing predicted concentrations to those observed in the maternal plasma during the second and third trimesters and in the maternal and umbilical cord plasma at delivery. Development of these models followed a standard workflow comprising the initial establishment of a non-pregnant PBPK model and the subsequent translation to pregnancy.

The pharmacokinetics of DTG predicted in pregnant non-laboring women was in good agreement with clinical data obtained at different stages of pregnancy (Fig. 3 and Table 4). While most PK parameters were adequately predicted, t_{max} in the second trimester was somewhat overestimated and AUC_{tau} underestimated in the third trimester (Table 4, Fig. 3). The reason for the decrease in t_{max} in the second (but not the third) trimester in vivo is yet unknown and further clinical studies strictly controlling for food intake could help to elucidate that point. The underestimation of AUC_{tau} in the third trimester could mainly be ascribed to an overestimation of total body clearance. Combined with the results from the sensitivity analysis on UGT1A1 induction (Fig. S4 of the ESM), this finding emphasizes that UGT1A1 induction may be lower than expected here and that changes in the fraction unbound are, at least for DTG, the main driver

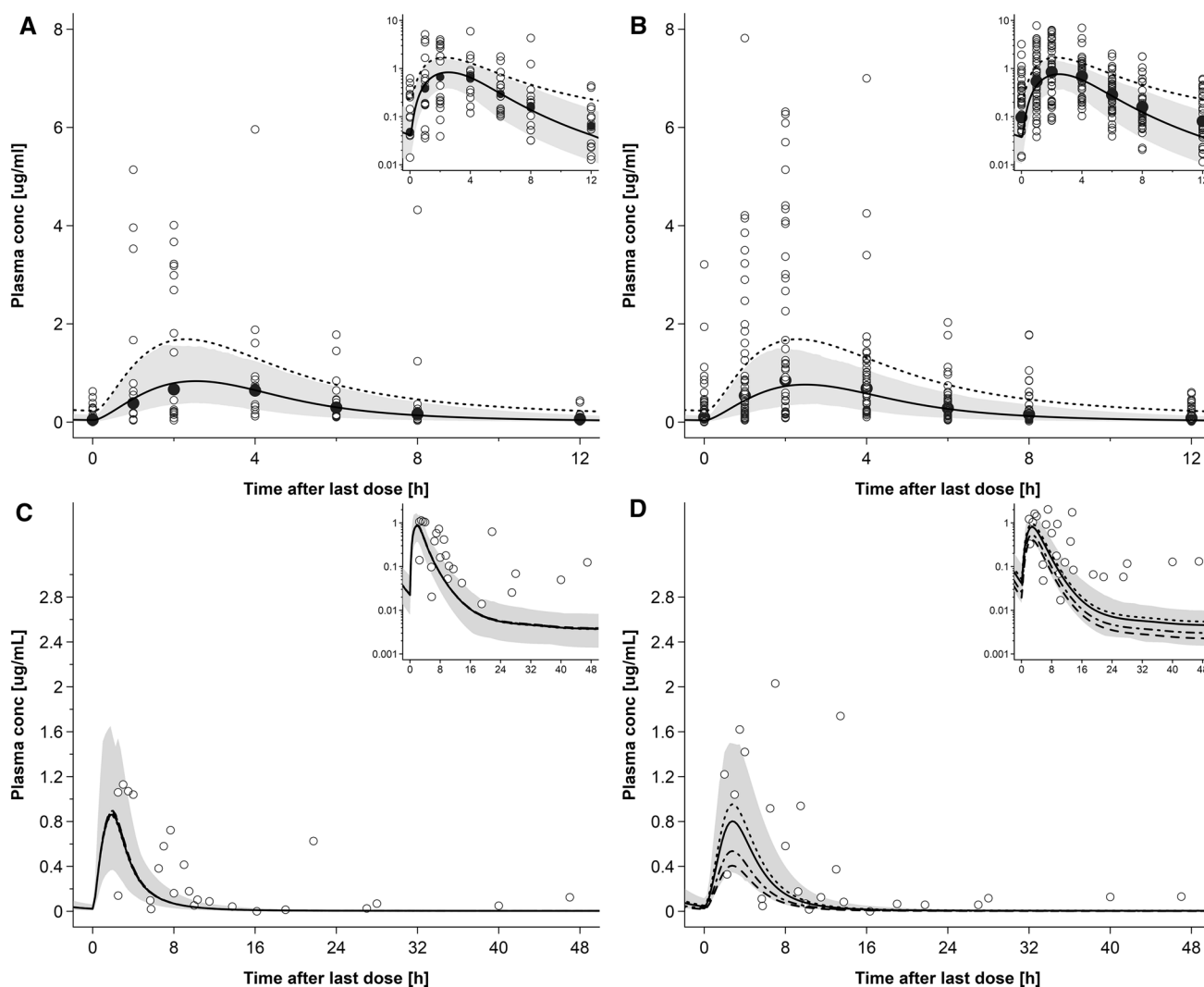


Fig. 5 Plasma concentration–time profiles of raltegravir following oral administration of 400 mg twice a day in pregnant women in steady state. Semi-log scale figures are given as an inset figure in the top-right corners. Observed steady-state in vivo data were taken from an in vivo study of IMPAACT P1026 [30]. **a** Raltegravir 400 mg twice a day in pregnant women in the second trimester. Empty circles and black circles represent individual concentrations and geometric mean concentration, respectively, taken from an in vivo study of IMPAACT P1026 [30]. The solid line represents the predicted geometric mean concentration and the shaded area the predicted 5th–95th percentile range; the dotted line represents the predicted geometric mean concentration of the non-pregnant population; **b** raltegravir 400 mg twice a day in pregnant women in the third trimester. Empty circles and black circles represent individual concentrations and geometric mean concentration, respectively, taken from an in vivo study of IMPAACT P1026 [30]. The solid line represents the predicted geometric mean concentration and the shaded area the predicted 5th–95th percentile range; the dotted line represents the predicted geometric mean concentration of the non-pregnant population; **c** raltegravir 400 mg twice a day in pregnant women with an average gestational age of 38 weeks at delivery. Empty circles represent individual con-

centration data in the maternal plasma taken from an in vivo study of IMPAACT P1026; [30] the lines represent the predicted mean concentrations in the maternal plasma using different placental partition coefficients calculated by different methods. The solid line represents the QSAR method; the dotted line represents the Poulin and Theil method; the dash-dot line represents the Rodgers and Rowland method; the dash line represents the PK-Sim standard method. The shaded area represents the predicted 5th–95th percentile range obtained from the model incorporating the QSAR-informed placental partition coefficient. **D**: raltegravir 400 mg twice a day in pregnant women with an average gestational age of 38 weeks at delivery. Empty circles represent individual concentration data in the umbilical vein taken from an in vivo study of IMPAACT P1026; [30] the lines represent the predicted mean concentrations in the umbilical vein using different placental partition coefficients calculated by different methods: the solid line represents the QSAR method; the dotted line represents the Poulin and Theil method; the dash-dot line represents the Rodgers and Rowland method; and the dash line represents the PK-Sim standard method. The shaded area represents the predicted 5th–95th percentile range obtained from the model incorporating the QSAR-informed placental partition coefficient

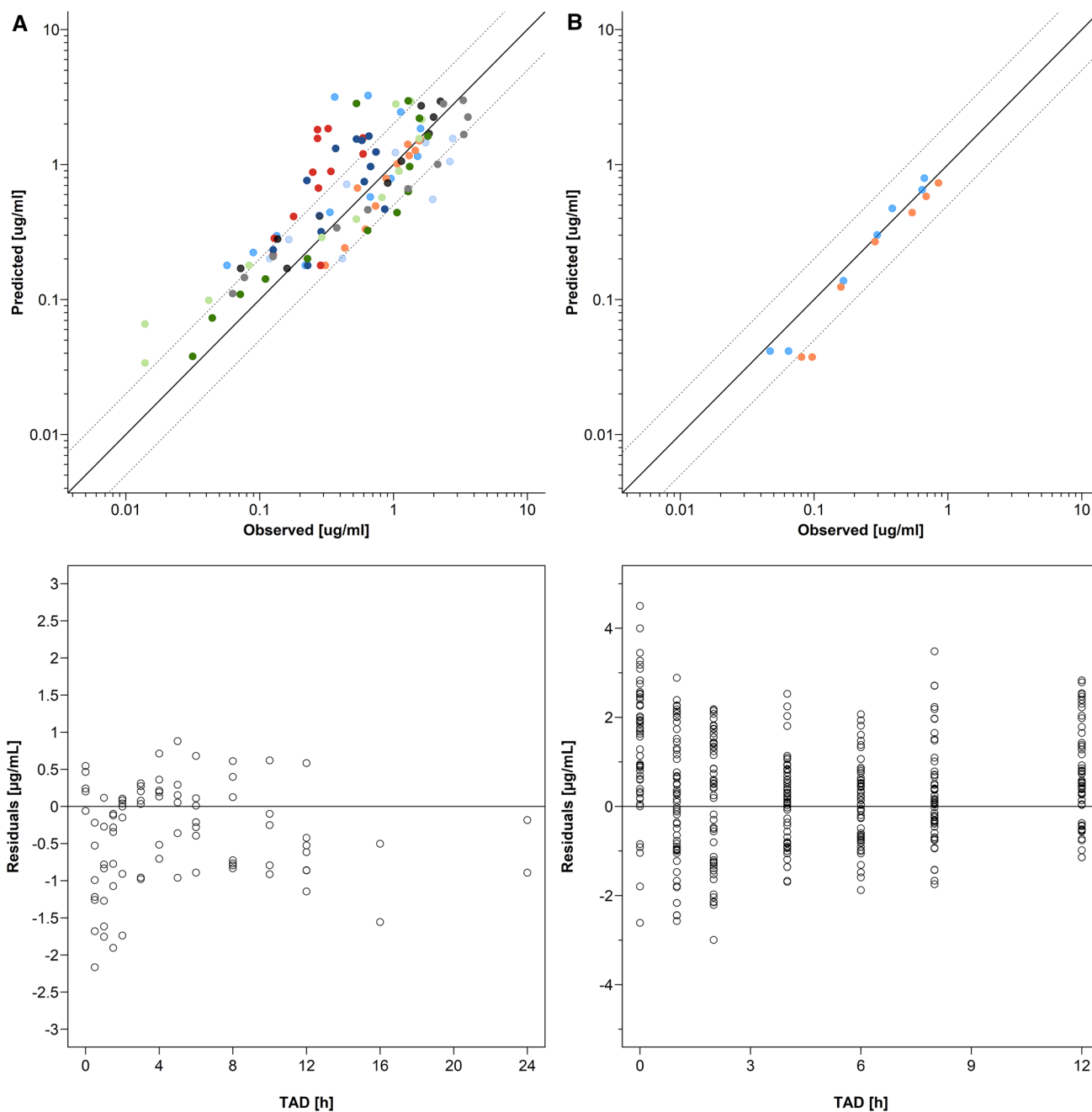


Fig. 6 Goodness-of-fit (GOF) and residuals vs time plots of raltegravir concentrations in non-pregnant subjects (a) and pregnant women (b). The solid line represents the line of identity and the dotted lines the two-fold error range. **a** Upper plot: GOF plot of geometric mean dolutegravir concentrations in non-pregnant populations. Single-dose study: bright green circles indicate the study by Iwamoto et al. (400-mg single dose) [78]; dark green circles indicate the study by Rhee et al. (400-mg single dose) [76]; grey circles indicate the study by Wenning et al. (400-mg single dose) [77]. Multiple-dose study: blue circles indicate the fasted group in the study by Brainard et al. (400-mg multiple dose) [79]; orange circles indicate the high-fat group in the study by Brainard et al. (400-mg multiple dose) [79]; dark blue circles indicate the high to moderate fat group in the study by Brain-

ard et al. (400-mg multiple dose) [79]; red circles indicate the low-fat group in the study by Brainard et al. (400-mg multiple dose) [79]; black circles indicate the study by Markowitz et al. (400-mg multiple dose) [75]. Sky blue circles indicate the group 1 in the study by Taburet et al. (400-mg multiple dose) [80]; light blue circles indicate the group 2 in the study by Taburet et al. (400-mg multiple dose) [80]; **b** upper plot: GOF plot of raltegravir in the pregnant population. Blue circles indicate geometric mean concentrations in women in the second trimester; orange circles indicate geometric mean concentrations in women in the third trimester. Lower plot: residuals vs time plot of raltegravir in the pregnant population. Empty circles represent the individual concentrations in the second and third trimesters

of increased total clearance, which is consistent with recent findings in the literature [46]. The pharmacokinetics of RAL were generally well predicted in pregnant non-laboring women (Fig. 5) and all mean PK parameters were predicted within a 1.33-fold error range (Table 4). However, variability was underestimated, especially in the first hours after drug administration, indicating that the model did not fully capture variability related to drug absorption.

UGT1A1 plays an important role in the metabolism of both DTG and RAL. While in vitro experiments support an increase in UGT1A1 expression mediated by rising progesterone levels during pregnancy [47], there is scarce information on quantitative changes in UGT1A1 expression during pregnancy in vivo. In a previous pregnancy PBPK model for acetaminophen (paracetamol), UGT1A1 was assumed to be induced by a factor of 1.75 in the second trimester and 1.92 in the third trimester [15] and these induction factors were incorporated here. Because of the relatively high uncertainty in these factors, a local sensitivity analysis was conducted (Fig. S4 of the ESM). While maternal pharmacokinetics of DTG was moderately sensitive to alterations in UGT1A1 expression, maternal pharmacokinetics of RAL was rather weakly affected by these alterations. Additional studies dedicatedly investigating UGT1A1 activity changes in pregnant women are needed to better define whether and to which extent UGT1A1 is induced during pregnancy. Clinical studies on different UGT1A1-metabolized drugs could be helpful to answer this question.

A key objective of this study was to predict pharmacokinetics of DTG and RAL in the maternal plasma and venous blood plasma of the umbilical cord at delivery. To this end, different approaches to inform placental transfer kinetics were tested. Specifically, D_{pl} (the placental diffusion clearance) was estimated from Caco-2 permeability [34] and $K_{fc:mp}$ (the fetal intracellular-to-maternal plasma partition coefficient in the placenta) was calculated either by previously reported methods for estimation of organ-to-plasma partition coefficients [37–41] or by a previously reported QSAR approach [42], assuming that the fetal–maternal blood concentration ratio can be used as surrogate for $K_{fc:mp}$. Hence, placental transfer was exclusively informed by in vitro and in silico methods. This has the strength to bypass the need for additional in vivo studies or ex-vivo experiments, such as the placental cotyledon perfusion experiment, but it also displays several shortcomings. For example, DTG is a substrate of P-glycoprotein (multidrug resistance protein 1), one of the major efflux transporters expressed in the placenta [48], and the effect of this transporter may not be consistently accounted for by the proposed approach for estimation of D_{pl} . Although drug transporters are present in Caco-2 cell lines, their expression may differ from that in placental cells and may not correlate with the placental protein amount in vivo [48], thereby distorting the

estimated D_{pl} value. Indeed, the limited data available seem to indicate that the expression of P-glycoprotein normalized to that of the housekeeping gene GAPDH (glyceraldehyde-3-phosphate dehydrogenase) is slightly higher in Caco-2 cells [49–52] than in the human term placenta [53, 54]. The higher P-glycoprotein expression in Caco-2 cells may consequently have contributed to an underestimation of D_{pl} . As shown in Fig. S6 of the ESM, D_{pl} was a sensitive model parameter for DTG but not for RAL. Unfortunately, the low number of observed data and the high variability therein, especially in the terminal phase, preclude any sound conclusion on whether the estimated D_{pl} for DTG should be higher. This illustrates the importance of developing new modeling approaches that delineate passive diffusion and active transport across the placenta.

The presented findings in Figs. 3d and 5d show that the various methods to estimate $K_{fc:mp}$ yield largely different predictions of umbilical vein concentrations. Given the relatively small size of the fetus, maternal plasma concentrations were barely affected by different $K_{fc:mp}$ values (Figs. 3c and 5c). In general, the small amount of clinical data hindered a thorough evaluation of these predictions and more data are clearly needed, ideally from different tissues (e.g., the maternal plasma, placenta, and umbilical vein) to better assess the predictive performance of these models. Nonetheless, keeping this limitation in mind, those models that informed $K_{fc:mp}$ via the Poulin and Theil method or the QSAR approach appeared to predict umbilical vein concentrations better than the other models. Umbilical vein concentrations of DTG appeared to be adequately predicted by these models (Fig. 3d), but RAL concentrations were generally underestimated, predominantly because maternal concentrations were also underestimated (Fig. 5c, d). This finding stresses the importance of the maternal pharmacokinetics on fetal drug exposure, indicating that the main elimination pathway of the fetus is transfer over the placenta back in the mother.

Raltegravir concentrations in the maternal plasma and umbilical vein were especially underestimated after 12 h (i.e., the dosing interval). One reason for the underestimation of maternal RAL plasma concentrations at delivery appeared to be the relatively fast absorption in the model. While the PBPK models for non-laboring women incorporated a fed state to reflect the fact that no restrictions on food intake were imposed in the clinical study, the PBPK model for laboring women incorporated the fasted state (assuming that food intake prior to the onset of labor and delivery is implausible). However, gastric passage of RAL (as well as DTG) was nonetheless delayed in the PBPK model at delivery because there is some evidence that gastric emptying and drug absorption from the gastrointestinal tract are slowed during labor [55–57]. Specifically, Whitehead et al. reported a three-fold delay in acetaminophen t_{max} in pregnant women ($n = 36$) during labor when compared with 2 h post-delivery

women ($n = 17$) [57]. Based on this observation, a three-fold delay in gastric emptying time was incorporated in the presented PBPK models for RAL and DTG at delivery, which may not have been enough to reflect the delay in drug absorption. Unfortunately, few clinical data are available for the first few hours after drug administration, which complicates a proper assessment of alterations in drug absorption around delivery. As discussed elsewhere in greater detail [9, 58], the effect of pregnancy on drug absorption is poorly understood. The potential effect of delivery, on top of that during pregnancy, further complicates the situation. Once informative clinical data are available, PBPK models applied to the peripartum period could investigate such effects and refine the understanding of physiological changes affecting drug absorption as well as other pharmacokinetic processes.

Ex vivo cotyledon perfusion experiments constitute another source of information for parameterization of placental transfer in PBPK models [59–61]. One of the advantages of these experiments is the possibility to estimate the fraction unbound of the compound in the placenta. Yet, data from these experiments are not always available for the studied drug and in other cases they may not translate into meaningful PBPK predictions. For example, although DTG was used in a previous ex-vivo cotyledon perfusion experiment, the transfer was observed to be very slow and apparent equilibrium concentrations were not reached after 3 h [62]. The authors discussed that one reason for the slow transfer could have been equal albumin levels in the maternal and fetal compartments. Indeed, differences in maternal and fetal protein binding can be critical determinants for placental transfer and equilibrium concentrations reached in steady state [63].

Because only the free drug fraction crosses the placenta, it can be expected that, for highly protein-bound drugs, an increase in the fetal fraction unbound is associated with a decrease in total concentrations at steady state because the bound drug concentration diminishes. Therefore, a maternal–fetal PBPK model should ideally consider such differences between the drug's fraction unbound in the maternal and fetal plasma. However, although technically possible in the herein presented model, little is known about changes in the fetal fraction unbound. While umbilical cord concentrations of fetal albumin and α -fetoprotein can in principle be easily measured from plasma samples obtained at delivery, it is unclear whether fetal albumin and α -fetoprotein display the same affinity to drugs as adult albumin. There is evidence that, compared to adult albumin, fetal albumin has a different binding affinity to several drugs [64, 65] and that α -fetoprotein lacks specific drug-binding sites [66, 67]. This complicates an estimation of a drug's unbound fraction in the fetal plasma. To correctly parameterize placental transfer of highly protein-bound drugs in PBPK models, clinical data of the fetal fraction unbound in vivo are clearly

needed. These data could then either be directly applied to inform PBPK models or to develop and train novel in silico approaches for prediction of the fetal fraction unbound.

On 18 May, 2018, the US FDA released a warning letter [68] that DTG may cause serious neural tube birth defects involving the brain, spine, and spinal cord. The preliminary observations were found in a study in Botswana in women who received DTG at the time of conception [68, 69]. Although the mechanism leading to the teratogenicity of DTG is not understood, one hypothesis is that DTG affects folic acid binding to the folate receptor- α , thereby reducing folic acid levels in the fetus [70]. As folic acid is essential for neural tube development, a reduction in folic acid can potentially cause neural tube defects in the fetus. According to in vitro results presented by Zamek-Gliszczyński et al. [70], free DTG concentrations of approximately 37 μM are associated with a 36% inhibition of folate receptor- α . To set these figures in the in vivo context, the presented PBPK model was extrapolated to the sixth gestational week while assuming an induction of UGT1A1 by 33% in the first trimester, as suggested previously [15]. Unbound DTG concentrations were then predicted in the maternal blood of the placenta. The maximum unbound DTG concentration predicted in steady state was 0.06 μM at the sixth gestational week. Using a simple Emax model fitted to the data reported by Zamek-Gliszczyński et al. [70] (fitted values are Emax: 1.0; EC50: 1276 μM), this DTG concentration translates into an inhibition of the folate receptor- α by approximately 7%. It should be noted, though, that this value is based on a model prediction that cannot be evaluated because of a lack of clinical data and it should therefore not be used to guide dosing decisions. Still, this example illustrates how PBPK modeling can theoretically contribute to support decision making for the use of DTG during pregnancy. This example also emphasizes the need for clinical data to support the confidence of model-based predictions.

5 Conclusions

The developed PBPK models successfully predicted the mean PK profile at different stages of pregnancy by leveraging prior knowledge about pregnancy-related effects on relevant physiological parameters and apparent enzyme activity. Importantly, umbilical vein concentrations were predicted by integrating information generated solely by in vitro or in silico techniques. This is the first study evaluating the applicability of standard equations for predicting the fetal–maternal partition coefficient in the placenta indicating that these equations yield largely different results. The presented models provide new mechanistic insights into the pharmacokinetics of RAL and DTG during pregnancy, which can be conceptually generalized and applied to other

drugs. The findings also stress the importance of measuring the unbound fraction of highly protein-bound drugs in both the maternal and fetal plasma when clinical trials are conducted in pregnant populations to facilitate the proper parameterization of PBPK models. Ultimately, verified PBPK models may be used to support informed decision making when clinical trials are designed in this frequently ignored population or when sound and consistent information from trials is lacking.

Acknowledgements The authors would like to thank Dr. Ibrahim Ince (Bayer AG) for providing the non-pregnant PBPK model for raltegravir via upload on OSP GitHub. The opinions expressed in this article are those of the authors and should not be interpreted as the position of the US Food and Drug Administration (FDA) or of the National Institutes of Health. No broader FDA policies or perspectives are intended nor should be inferred. The FDA does not recommend any specific PBPK software.

Compliance with Ethical Standards

Conflict of interest Xiaomei I. Liu, Jeremiah D. Momper, Natella Y. Rakhmanina, Dionna J. Green, Gilbert J. Burckart, Tim R. Cressey, Mark Mirochnick, Brookie M. Best, John N. van den Anker, and André Dallmann have no potential conflicts of interest with respect to the research, authorship, and/or publication of this article. André Dallmann is an employee of Bayer AG and involved in OSP software development. The results from this study were presented in part at the American College of Clinical Pharmacology Annual Meeting, Washington, DC, September 2018.

Funding Overall support for the International Maternal Pediatric Adolescent AIDS Clinical Trials Network (IMPAACT) was provided by the National Institute of Allergy and Infectious Diseases with co-funding from the Eunice Kennedy Shriver National Institute of Child Health and Human Development (NICHD) and the National Institute of Mental Health, all components of the National Institutes of Health (NIH), under Award Numbers UM1AI068632 (IMPAACT LOC), UM1AI068616 (IMPAACT SDMC), and UM1AI106716 (IMPAACT LC), and by NICHD contract number HHSN275201800001I. The NIH awards numbers 5T32HD087969-03 and 5T32HD087969-02 also support this project.

References

1. Taylor AW, Nesheim SR, Zhang X, Song R, Fitzharris LF, Lampe MA, et al. Estimated perinatal HIV infection among infants born in the United States, 2002–2013. *JAMA Pediatr.* 2017;171(5):435–42.
2. Nesheim SR, Fitzharris LF, Lampe MA, Gray KM. Reconsidering the number of women with HIV infection who give birth annually in the United States. *Public Health Rep.* 2018;133(6):637–43.
3. Nesheim S, Taylor A, Lampe MA, Kilmarx PH, Fitz Harris L, Whitmore S, et al. A framework for elimination of perinatal transmission of HIV in the United States. *Pediatrics.* 2012;130(4):738–44.
4. Caritis SN, Bastian JR, Zhang H, Kalluri H, English D, England M, et al. An evidence-based recommendation to increase the dosing frequency of buprenorphine during pregnancy. *Am J Obstet Gynecol.* 2017;217(4):459.e1–6.
5. Krishna R, East L, Larson P, Valiathan C, Deschamps K, Luk JA, et al. Atazanavir increases the plasma concentrations of 1200 mg raltegravir dose. *Biopharm Drug Dispos.* 2016;37(9):533–41.
6. Rahangdale L, Cates J, Potter J, Badell ML, Seidman D, Miller ES, et al. Integrase inhibitors in late pregnancy and rapid HIV viral load reduction. *Am J Obstet Gynecol.* 2016;214(3):385.e1–7.
7. World Health Organization. Update of recommendations on first- and second-line antiretroviral regimens. <https://www.who.int/hiv/pub/arv/arv-update-2019-policy/en/>. Accessed 18 Nov 2019.
8. National Institutes of Health. Recommendations for the use of antiretroviral drugs in pregnant women with HIV infection and interventions to reduce perinatal HIV transmission in the United States. 2018. <https://aidsinfo.nih.gov/guidelines/html/3/perinatal/0>. Accessed 18 Nov 2019.
9. Dallmann A, Pfister M, Van Den Anker J, Eissing T. Physiologically based pharmacokinetic modeling in pregnancy: a systematic review of published models. *Clin Pharmacol Ther.* 2018;104(6):1110–24.
10. Yap CW. PaDEL-descriptor: an open source software to calculate molecular descriptors and fingerprints. *J Comput Chem.* 2011;32(7):1466–74.
11. Dallmann A, Solodenko J, Ince I, Eissing T. Applied concepts in PBPK modeling: how to extend an open systems pharmacology model to the special population of pregnant women. *CPT Pharmacomet Syst Pharmacol.* 2018;7(7):419–31.
12. Reese MJ, Savina PM, Generaux GT, Tracey H, Humphreys JE, Kanaoka E, et al. In vitro investigations into the roles of drug transporters and metabolizing enzymes in the disposition and drug interactions of dolutegravir, a HIV integrase inhibitor. *Drug Metab Dispos.* 2013;41(2):353–61.
13. Dallmann A, Ince I, Meyer M, Willmann S, Eissing T, Hempel G. Gestation-specific changes in the anatomy and physiology of healthy pregnant women: an extended repository of model parameters for physiologically based pharmacokinetic modeling in pregnancy. *Clin Pharmacokinet.* 2017;56(11):1303–30.
14. Dallmann A, Ince I, Coboeken K, Eissing T, Hempel G. A physiologically based pharmacokinetic model for pregnant women to predict the pharmacokinetics of drugs metabolized via several enzymatic pathways. *Clin Pharmacokinet.* 2018;57(6):749–68.
15. Mian P, Van Den Anker JN, Van Calsteren K, Annaert P, Tibboel D, Pfister M, et al. Physiologically based pharmacokinetic modeling to characterize acetaminophen pharmacokinetics and *N*-acetyl-*p*-benzoquinone imine (NAPQI) formation in non-pregnant and pregnant women. *Clin Pharmacokinet.* 2020;59(1):97–110. <https://doi.org/10.1007/s40262-019-00799-5>.
16. Center for Drug Evaluation and Research. Clinical pharmacology and biopharmaceutics review (s). https://www.accessdata.fda.gov/drugsatfda_docs/nda/2013/204790Orig1s000ClinPharmR.pdf. Accessed 8 Oct 2019.
17. Castellino S, Moss L, Wagner D, Borland J, Song I, Chen S, et al. Metabolism, excretion, and mass balance of the HIV-1 integrase inhibitor dolutegravir in humans. *Antimicrob Agents Chemother.* 2013;57(8):3536–46.
18. Dooley KE, Sayre P, Borland J, Purdy E, Chen S, Song I, et al. Safety, tolerability, and pharmacokinetics of the HIV integrase inhibitor dolutegravir given twice daily with rifampin or once daily with rifabutin: results of a phase 1 study among healthy subjects. *J Acquir Immune Defic Syndr.* 2013;62(1):21–7.
19. Song IH, Borland J, Savina PM, Chen S, Patel P, Wajima T, et al. Pharmacokinetics of single-dose dolutegravir in HIV-seronegative subjects with moderate hepatic impairment compared to healthy matched controls. *Clin Pharmacol Drug Dev.* 2013;2(4):342–8.
20. Song I, Weller S, Patel J, Borland J, Wynne B, Choukour M, et al. Effect of carbamazepine on dolutegravir pharmacokinetics and dosing recommendation. *Eur J Clin Pharmacol.* 2016;72(6):665–70.

21. Song I, Borland J, Chen S, Patel P, Wajima T, Peppercorn A, et al. Effect of food on the pharmacokinetics of the integrase inhibitor dolutegravir. *Antimicrob Agents Chemother.* 2012;56(3):1627–9.
22. Weller S, Borland J, Chen S, Johnson M, Savina P, Wynne B, et al. Pharmacokinetics of dolutegravir in HIV-seronegative subjects with severe renal impairment. *Eur J Clin Pharmacol.* 2014;70(1):29–35.
23. Ford SL, Gould E, Chen S, Margolis D, Spreen W, Crauwels H, et al. Lack of pharmacokinetic interaction between rilpivirine and integrase inhibitors dolutegravir and GSK1265744. *Antimicrob Agents Chemother.* 2013;57(11):5472–7.
24. Johnson M, Borland J, Chen S, Savina P, Wynne B, Piscitelli S. Effects of boceprevir and telaprevir on the pharmacokinetics of dolutegravir. *Br J Clin Pharmacol.* 2014;78(5):1043–9.
25. Wang X, Cerrone M, Ferretti F, Castrillo N, Maartens G, McClure M, et al. Pharmacokinetics of dolutegravir 100 mg once daily with rifampicin. *Int J Antimicrob Agents.* 2019;54(2):202–6.
26. Min S, Song I, Borland J, Chen S, Lou Y, Fujiwara T, et al. Pharmacokinetics and safety of S/GSK1349572, a next-generation HIV integrase inhibitor, in healthy volunteers. *Antimicrob Agents Chemother.* 2010;54(1):254–8.
27. Kassahun K, Mcintosh I, Cui D, Hreniuk D, Merschman S, Lassester K, et al. Metabolism and disposition in humans of raltegravir (MK-0518), an anti-AIDS drug targeting the human immunodeficiency virus 1 integrase enzyme. *Drug Metab Dispos.* 2007;35(9):1657–63.
28. Laufer R, Paz OG, Di Marco A, Bonelli F, Monteagudo E, Summa V, et al. Quantitative prediction of human clearance guiding the development of raltegravir (MK-0518, isentress) and related HIV integrase inhibitors. *Drug Metab Dispos.* 2009;37(4):873–83.
29. Mulligan N, Best BM, Wang J, Capparelli EV, Stek A, Barr E, et al. Dolutegravir pharmacokinetics in pregnant and postpartum women living with HIV. *AIDS.* 2018;32(6):729–37.
30. Watts DH, Stek A, Best BM, Wang J, Capparelli EV, Cressey TR, et al. Raltegravir pharmacokinetics during pregnancy. *J Acquir Immune Defic Syndr.* 2014;67(4):375–81.
31. Waitt C, Orrell C, Walimbwa S, Singh Y, Kintu K, Simmons B, et al. Safety and pharmacokinetics of dolutegravir in pregnant mothers with HIV infection and their neonates: a randomised trial (DolPHIN-1 study). *PLoS Med.* 2019;16(9):e1002895.
32. Blonk MI, Colbers AP, Hidalgo-Tenorio C, Kabeya K, Wezsacker K, Haberl AE, et al. Raltegravir in HIV-1-infected pregnant women: pharmacokinetics, safety, and efficacy. *Clin Infect Dis.* 2015;61(5):809–16.
33. Dallmann A, Ince I, Solodenko J, Meyer M, Willmann S, Eissing T, et al. Physiologically based pharmacokinetic modeling of renally cleared drugs in pregnant women. *Clin Pharmacokinet.* 2017;56(12):1525–41.
34. Zhang Z, Unadkat JD. Development of a novel maternal–fetal physiologically based pharmacokinetic model II: verification of the model for passive placental permeability drugs. *Drug Metab Dispos.* 2017;45(8):939–46.
35. Griessinger JA, Hauptstein S, Laffleur F, Netsomboon K, Bernkop-Schnurch A. Evaluation of the impact of multivalent metal ions on the permeation behavior of dolutegravir sodium. *Drug Dev Ind Pharm.* 2016;42(7):1118–26.
36. Moss DM, Kwan WS, Liptrott NJ, Smith DL, Siccardi M, Khoo SH, et al. Raltegravir is a substrate for SLC22A6: a putative mechanism for the interaction between raltegravir and tenofovir. *Antimicrob Agents Chemother.* 2011;55(2):879–87.
37. Open Systems Pharmacology: Compounds: Definition and Work Flows. <https://docs.open-systems-pharmacology.org/working-with-pk-sim/pk-sim-documentation/pk-sim-compounds-definition-and-work-flow#adme-properties>. Accessed 29 Feb 2020.
38. Poulin P, Schoenlein K, Theil FP. Prediction of adipose tissue: plasma partition coefficients for structurally unrelated drugs. *J Pharm Sci.* 2001;90(4):436–47.
39. Poulin P, Theil FP. Prediction of pharmacokinetics prior to in vivo studies. 1. Mechanism-based prediction of volume of distribution. *J Pharm Sci.* 2002;91(1):129–56.
40. Rodgers T, Leahy D, Rowland M. Physiologically based pharmacokinetic modeling 1: predicting the tissue distribution of moderate-to-strong bases. *J Pharm Sci.* 2005;94(6):1259–76.
41. Rodgers T, Rowland M. Physiologically based pharmacokinetic modelling 2: predicting the tissue distribution of acids, very weak bases, neutrals and zwitterions. *J Pharm Sci.* 2006;95(6):1238–57.
42. Takaku T, Nagahori H, Sogame Y, Takagi T. Quantitative structure-activity relationship model for the fetal–maternal blood concentration ratio of chemicals in humans. *Biol Pharm Bull.* 2015;38(6):930–4.
43. Nishimura M, Yaguti H, Yoshitsugu H, Naito S, Satoh T. Tissue distribution of mRNA expression of human cytochrome P450 isoforms assessed by high-sensitivity real-time reverse transcription PCR. *Yakugaku Zasshi.* 2003;123(5):369–75.
44. Kawade N, Onishi S. The prenatal and postnatal development of UDP-glucuronyltransferase activity towards bilirubin and the effect of premature birth on this activity in the human liver. *Biochem J.* 1981;196(1):257–60.
45. Collier AC, Thevenon AD, Goh W, Hiraoka M, Kendal-Wright CE. Placental profiling of UGT1A enzyme expression and activity and interactions with preeclampsia at term. *Eur J Drug Metab Pharmacokinet.* 2015;40(4):471–80.
46. Bollen P, Freriksen J, Konopnicki D, Wezsacker K, Hidalgo Tenorio C, Molto J, et al. The effect of pregnancy on the pharmacokinetics of total and unbound dolutegravir and its main metabolite in women living with human immunodeficiency virus. *Clin Infect Dis.* 2020. <https://doi.org/10.1093/cid/ciaa006>.
47. Jeong H, Choi S, Song JW, Chen H, Fischer JH. Regulation of UDP-glucuronosyltransferase (UGT) 1A1 by progesterone and its impact on labetalol elimination. *Xenobiotica.* 2008;38(1):62–75.
48. Dallmann A, Liu XI, Burckart GJ, Van Den Anker J. Drug transporters expressed in the human placenta and models for studying maternal–fetal drug transfer. *J Clin Pharmacol.* 2019;59(Suppl. 1):S70–81.
49. Pfrunder A, Gutmann H, Beglinger C, Drewe J. Gene expression of CYP3A4, ABC-transporters (MDR1 and MRP1-MRP5) and hPXR in three different human colon carcinoma cell lines. *J Pharm Pharmacol.* 2003;55(1):59–66.
50. Nakamura T, Sakaeda T, Ohmoto N, Moriya Y, Komoto C, Shirakawa T, et al. Gene expression profiles of ABC transporters and cytochrome P450 3A in Caco-2 and human colorectal cancer cell lines. *Pharm Res.* 2003;20(2):324–7.
51. Zrieki A, Farinotti R, Buyse M. Cyclooxygenase inhibitors down regulate P-glycoprotein in human colorectal Caco-2 cell line. *Pharm Res.* 2008;25(9):1991–2001.
52. Yano K, Shimizu S, Tomono T, Ogihara T. Gastrointestinal hormone cholecystokinin increases P-glycoprotein membrane localization and transport activity in Caco-2 cells. *J Pharm Sci.* 2017;106(9):2650–6.
53. Sun M, Kingdom J, Baczyk D, Lye SJ, Matthews SG, Gibb W. Expression of the multidrug resistance P-glycoprotein, (ABCB1 glycoprotein) in the human placenta decreases with advancing gestation. *Placenta.* 2006;27(6–7):602–9.
54. Wang C, Li H, Luo C, Li Y, Zhang Y, Yun D, et al. The effect of maternal obesity on the expression and functionality of placental P-glycoprotein: implications in the individualized transplacental digoxin treatment for fetal heart failure. *Placenta.* 2015;36(10):1138–47.

55. Bataille A, Rousset J, Marret E, Bonnet F. Ultrasonographic evaluation of gastric content during labour under epidural analgesia: a prospective cohort study. *Br J Anaesth*. 2014;112(4):703–7.
56. Davison JS, Davison MC, Hay DM. Gastric emptying time in late pregnancy and labour. *J Obstet Gynaecol Br Commonw*. 1970;77(1):37–41.
57. Whitehead EM, Smith M, Dean Y, O'sullivan G. An evaluation of gastric emptying times in pregnancy and the puerperium. *Anaesthesia*. 1993;48(1):53–7.
58. Stillhart C, Vucicevic K, Augustijns P, Basit AW, Batchelor H, Flanagan TR, et al. Impact of gastrointestinal physiology on drug absorption in special populations: an UNGAP review. *Eur J Pharm Sci*. 2020;147:105280.
59. De Sousa MM, Hirt D, Vinot C, Valade E, Lui G, Pressiat C, et al. Prediction of human fetal pharmacokinetics using ex vivo human placenta perfusion studies and physiologically based models. *Br J Clin Pharmacol*. 2016;81(4):646–57.
60. Schalkwijk S, Buaben AO, Freriksen JJM, Colbers AP, Burger DM, Greupink R, et al. Prediction of fetal darunavir exposure by integrating human ex-vivo placental transfer and physiologically based pharmacokinetic modeling. *Clin Pharmacokinet*. 2018;57(6):705–16.
61. Liu XI, Momper JD, Rakhmanina N, Van Den Anker JN, Green DJ, Burckart GJ, et al. Physiologically based pharmacokinetic models to predict maternal pharmacokinetics and fetal exposure to emtricitabine and acyclovir. *J Clin Pharmacol*. 2020;60(2):240–55.
62. Schalkwijk S, Greupink R, Colbers AP, Wouterse AC, Verweij VG, Van Drongelen J, et al. Placental transfer of the HIV integrase inhibitor dolutegravir in an ex vivo human cotyledon perfusion model. *J Antimicrob Chemother*. 2016;71(2):480–3.
63. Hill MD, Abramson FP. The significance of plasma protein binding on the fetal/maternal distribution of drugs at steady-state. *Clin Pharmacokinet*. 1988;14(3):156–70.
64. Chignell CF, Vesell ES, Starkweather DK, Berlin CM. The binding of sulfaphenazole to fetal, neonatal, and adult human plasma albumin. *Clin Pharmacol Ther*. 1971;12(6):897–901.
65. Krasner J, Giacoia GP, Yaffe SJ. Drug–protein binding in the newborn infant. *Ann N Y Acad Sci*. 1973;226:101–14.
66. Herve F, Rajkowski K, Martin MT, Dessen P, Cittanova N. Drug-binding properties of rat alpha 1-foetoprotein: binding of warfarin, phenylbutazone, azapropazone, diazepam, digitoxin and cholic acid. *Biochem J*. 1984;221(2):401–6.
67. Hirano K, Watanabe Y, Adachi T, Ito Y, Sugiura M. Drug-binding properties of human alpha-foetoprotein. *Biochem J*. 1985;231(1):189–91.
68. US Food and Drug Administration. FDA drug safety communication: FDA to evaluate potential risk of neural tube birth defects with HIV medicine dolutegravir (Juluca, Tivicay, Triumeq). 2018. <https://www.fda.gov/Drugs/DrugSafety/ucm608112.htm>. Accessed 25 Jun 2018.
69. WHO. Potential safety issue affecting women living with HIV using dolutegravir at the time of conception. 2018. https://www.who.int/medicines/publications/drugalerts/Statement_on_DTG_18May_2018final.pdf. Accessed 11 Nov 2019.
70. Zamek-Gliszczyński MJ, Zhang X, Mudunuru J, Du Y, Chen JL, Taskar KS, et al. Clinical extrapolation of the effects of dolutegravir and other HIV integrase inhibitors on folate transport pathways. *Drug Metab Dispos*. 2019;47(8):890–8.
71. Moss DM, Siccardi M, Murphy M, Piperakis MM, Khoo SH, Back DJ, et al. Divalent metals and pH alter raltegravir disposition in vitro. *Antimicrob Agents Chemother*. 2012;56(6):3020–6.
72. Moss DM, Siccardi M, Back DJ, Owen A. Predicting intestinal absorption of raltegravir using a population-based ADME simulation. *J Antimicrob Chemother*. 2013;68(7):1627–34.
73. Iwamoto M, Wenning LA, Petry AS, Laethem M, De Smet M, Kost JT, et al. Minimal effects of ritonavir and efavirenz on the pharmacokinetics of raltegravir. *Antimicrob Agents Chemother*. 2008;52(12):4338–433.
74. Iwamoto M, Wenning LA, Petry AS, Laethem M, De Smet M, Kost JT, et al. Safety, tolerability, and pharmacokinetics of raltegravir after single and multiple doses in healthy subjects. *Clin Pharmacol Ther*. 2008;83(2):293–9.
75. Markowitz M, Morales-Ramirez JO, Nguyen BY, Kovacs CM, Steigbigel RT, Cooper DA, et al. Antiretroviral activity, pharmacokinetics, and tolerability of MK-0518, a novel inhibitor of HIV-1 integrase, dosed as monotherapy for 10 days in treatment-naïve HIV-1-infected individuals. *J Acquir Immune Defic Syndr*. 2006;43(5):509–15.
76. Rhee EG, Rizk ML, Brainard DM, Gendrano IN 3rd, Jin B, Wenning LA, et al. A pharmacokinetic comparison of adult and paediatric formulations of raltegravir in healthy adults. *Antivir Ther*. 2014;19(6):619–24.
77. Wenning LA, Hanley WD, Brainard DM, Petry AS, Ghosh K, Jin B, et al. Effect of rifampin, a potent inducer of drug-metabolizing enzymes, on the pharmacokinetics of raltegravir. *Antimicrob Agents Chemother*. 2009;53(7):2852–6.
78. Iwamoto M, Wenning LA, Nguyen BY, Teppler H, Moreau AR, Rhodes RR, et al. Effects of omeprazole on plasma levels of raltegravir. *Clin Infect Dis*. 2009;48(4):489–92.
79. Brainard DM, Friedman EJ, Jin B, Breidinger SA, Tillan MD, Wenning LA, et al. Effect of low-, moderate-, and high-fat meals on raltegravir pharmacokinetics. *J Clin Pharmacol*. 2011;51(3):422–7.
80. Taburet AM, Sauvageon H, Grinsztejn B, Assuied A, Veloso V, Pilotto JH, et al. Pharmacokinetics of raltegravir in HIV-infected patients on rifampicin-based antitubercular therapy. *Clin Infect Dis*. 2015;61(8):1328–35.